Mechanical Systems and Signal Processing (1998) **12**(4), 571–588
Article No. pg970124

INTELLIGENT JOINT FAULT DIAGNOSIS OF INDUSTRIAL ROBOTS

M.-C. Pan*, H. Van Brussel and P. Sas

Department of Mechanical Engineering, Katholieke Universiteit Leuven, Celestijnenlaan 300B, B-3001 Leuven, Belgium

(Received September 1996, accepted for revision July 1997)

The dynamic behaviour of high-performance mechanical systems such as robots is strongly influenced by the characteristics of the link joints. Joint backlash as a result of wear due to severe stress imposed on the transmission system degrades the robot performance. This paper presents a systematic methodology to diagnose the joint-backlash of a robot by monitoring its vibration response during normal operations. To indicate the reversal of motion of a robot link, and to characterise the spectral patterns of vibration signatures, non-stationary time–frequency analysis algorithms have been employed, which illustrate the signature in a simultaneous time–frequency plane. Significant features are extracted from time domain analysis (probability density moments), and from time–frequency domain analysis (local energy calculations). Artificial neural networks are used as tools for pattern recognition. Experimental results show that the proposed techniques can analyse single-joint backlash quantitatively. Moreover, the described methods also allow to single out backlash in the individual joints in case of multiple-joint backlash.

1. INTRODUCTION

Well-maintained machines hold tolerances within limits, and raise consistency and quality of the product. In an industrial operation such as precision assembly, welding or drilling, the end-effector of a robot must move to the specific point, execute the task, withdraw, and then return to the same place on command. To fulfill the task, each joint requires a transmission, either geared or via ball-screws to provide adequate torque to drive the end-effector at the required speed. The work load can impose severe stresses on the transmission system which will inevitably cause friction, wear, lead to increased backlash, and eventually degrade robot performance.

Much research has aimed at fault detection and diagnosis of machines based on artificial neural networks (ANNs). As to the investigation of joint degradation on robots, Lee and Kramer [1] developed a cerebellar model articulation controller neural network-based reasoning tool to analyse the consistency of the machine behaviour based on the locations of weights in a look-up table. Poor positioning accuracy and path straightness were used as symptoms of the degraded performance. To detect joint faults on robots by monitoring vibration response, Bicker and Daadbin [2] analysed dynamically the characteristics of the links by powering up the robot link. An experimental programme was carried out to establish the change in the vibration spectra resulting from induced faults in the transmission of the elbow joint on a PUMA 560 robot. However, the subtle shift of peak

* Dr Pan currently works as a senior researcher with the R&D division of Sangyang Industry Co., Ltd., Taipei, Taiwan, R.O.C.

0888–3270/98/040571 + 18 $30.00/0

amplitude at some frequency bands for various backlash conditions was not reliable enough to be used as a criterion for fault diagnosis. The results obtained in Bicker and Daadbin's research can be explained as follows. Backlash can influence the vibration response of the robot elements during normal operations. However, when a conventional spectrum analysis is used to process the vibration signatures, the characteristics of backlash at the reversal of motion can be averaged out over the whole cycle. Therefore, the distinct differences between the signatures for different fault conditions cannot be identified. To obtain more detailed spectral information, Feldman and Braun's study [3], which focused on the modeling of non-linear vibration systems with backlash, gave simulation results which identified non-linear system parameters via instantaneous frequency applying Wigner–Ville techniques.

Besides the drawbacks of using conventional spectra analysis to process signals with transient nature, in general it is not well designed for the fault diagnosis of robots in a workshop; particularly when the data acquisition system is separated from the control system of a robot, as the starting (reference) point for each measurement can be different. Moreover, when some relevant information like the velocity of links cannot be obtained, it can be difficult to find the reversal of motion of a robot link. Considering on-line, real-time fault detection, without production interrupt, there is a great demand for developing a reliable diagnosis procedure to monitor the operation of robots based on signals measured during normal operations. To cope with these difficulties, the approaches proposed in this paper consist of three phases.

- In the preprocessing phase, spectrograms, which are closely related to the energy distribution of signals, are employed to indicate the reversal of motion of robot links. Hence, the interval of motion-reversal can be set.
- In the processing phase, the spectral patterns of vibration signatures are characterised by using smoothed Wigner–Ville distributions (SWVDs). One can tunes the time–frequency (TF) resolution of SWVDs flexibly to characterise and enhance the differences in the TF plane. SWVDs can help to extract features, e.g. the local energy in a subregion of the TF plane. Spectrograms are used to calculate the local energy. Some other significant features, such as kurtosis and variance during the interval of the reversal of motion, are also calculated.
- In the postprocessing phase, a supervised learning scheme with a modified backpropagation algorithm [4] is used as the engine of the ANNs.

In the experimental programme, the proposed methods have been applied initially to recognise different degrees of single backlash in the wrist swivel joint (joint 6) of an industrial robot. The single backlash in the wrist roll joint (joint 4) is also detected. Consecutively, the recognition procedure have been generalised to diagnose faults when both joints 6 and 4 are working simultaneously.

2. THEORETICAL BACKGROUND

The proposed automated robot-joint condition monitoring procedure consists of three major phases: (i) measurement segmentation and indication of the reversal of joint-motion (preprocessing); (ii) data processing including feature extraction (processing); and (iii) pattern classification and decision making (postprocessing).

2.1. NON-STATIONARY TF ANALYSIS

The vibrations measured at the end-effector of a robot with joint-backlash are referred to as non-stationary (transient and time varying), in contrast to stationary rotary machines

such as pumps, compressors, etc. The non-stationary phenomena can be attributed to two reasons, i.e. the characters of joint motion, and joint backlash. A typical motion cycle, which is time-varying, consists of an acceleration from the initial position, a movement with constant speed, and finally deceleration towards the end position. On the other hand, backlash can cause undesired vibration phenomena (impact transients) at the reversal of motion. By means of TF analysis [5, 6], the spectral components are identified in a TF plane, and therefore certain temporary vibration events can be characterised.

In this section, a number of TF analysis techniques, such as spectrograms, pseudo-WVDs (PWVDs) and SWVDs are introduced. In the fault diagnosis of robot joints, spectrograms are used both to locate the reversal of joint motion in the preprocessing phase, and to calculate the local energy feature in the processing phase. The SWVDs of vibration waveforms corresponding to different fault conditions are calculated and used to select features in the TF plane.

Let $f(t)$ be an analysed signal, and $g(t)$ a weighting window function. The spectrogram can be defined as [7, 8]:

$$SPE_{Z_f}^{(g)}(t, \omega) = \left| \int_{t'} Z_f(t') g^*(t' - t)\, \mathrm{e}^{-j\omega t'}\, \mathrm{d}t' \right|^2, \tag{1}$$

which is the squared magnitude of a windowed Fourier transform. As only the spectrum in the positive frequency is interested, the analytical form of $f(t)$, $Z_f(t)$, is applied. The TF representation (TFR) of a spectrogram exhibits proportionally the energy distribution in a TF plane [8]. A trade-off is required between the time and frequency resolution according to the uncertainty principle. To remove this effect, one can consider another class of TFR, i.e. Wigner–Ville distributions [9–11],

$$WV_{Z_f}(t, \omega) = \int_{-\infty}^{\infty} Z_f\left(t + \frac{\tau}{2}\right) Z_f^*\left(t - \frac{\tau}{2}\right) \mathrm{e}^{-j\omega\tau}\, \mathrm{d}\tau. \tag{2}$$

To avoid aliasing, the analytical form of a signal, $Z_f(t)$, is used. Otherwise, a sampling frequency, which is twice as high as that used for a Fourier transform, has to be used [12]. For computational purposes, it is in general necessary to weight the signal $Z_f(t)$ by a function $w(t)$ before evaluating the WVD, i.e. $Z_{f_t}(\tau) = Z_f(\tau) w(\tau - t)$. Therefore, equation (2) becomes

$$WV_{Z_f}(\tau, \omega) = \int_{-\infty}^{\infty} \left[Z_f\left(\tau + \frac{\eta}{2}\right) w\left(\tau - t + \frac{\tau}{2}\right) \right] \left[Z_f^*\left(\tau - \frac{\eta}{2}\right) w^*\left(\tau - t - \frac{\tau}{2}\right) \right] \mathrm{e}^{-j\omega\eta}\, \mathrm{d}\eta. \tag{3}$$

At a specific time t, the result is known as the pseudo-WVD, and can be written as

$$\tilde{W}V_{Z_f}(t, \omega) \equiv WV_{Z_{f_t}}(\tau, \omega)|_{\tau = t} = \int_{-\infty}^{\infty} Z_f\left(t + \frac{\eta}{2}\right) Z_f^*\left(t - \frac{\eta}{2}\right) w\left(\frac{\eta}{2}\right) w^*\left(\frac{-\eta}{2}\right) \mathrm{d}\eta. \tag{4}$$

Compared with spectrograms, PWVDs can offer good TF resolution. However, PWVDs yield interferences between each two spectral components, which can mask important spectral information. To depress those unwanted artifacts, one can smooth the WVD by

using double convolution [13, 14]. When the smoothing function is in the class of separable function, the smoothed Wigner–Ville distribution can be expressed as

$$\tilde{\tilde{W}}V_{Z_f}(t,\omega)=\int_{-\infty}^{\infty}\left[\int_{-\infty}^{\infty}Z_f\left(t-\tau+\frac{\tau'}{2}\right)Z_f^*\left(t-\tau+\frac{\tau'}{2}\right)g_1(\tau)\,\mathrm{d}\tau\right]g_2(\tau')\,\mathrm{e}^{-j\omega\tau'}\,\mathrm{d}\tau', \quad (5)$$

where $g_1(\tau)$ and $g_2(\tau')$ are the time- and frequency-smoothing windows, respectively. If inseparable, the yielded SWVD will be identical to the spectrogram [15], i.e. the squared amplitude of the windowed Fourier transform of $Z_f(t)$ using $g(t)$ as a weighting window. Then, it loses the significance of flexibly tuning the time and the frequency resolution. Compared with equation (1), there are more freedoms in equation (5) to choose the time-smoothing window as well as the frequency smoothing window.

2.2. FEATURE EXTRACTION

Before training sets are fed into an ANN, the most significant features which show a high sensitivity to joint faults should be extracted. In this study, the following features are considered.

2.2.1. *Variance (during the interval of motion reversal)*

A zero-acceleration region followed by an impact transient can be observed in the waveform resulting from a backlash condition. It will yield a smaller variance value. The variance can identify the differences for a joint in good condition or in fault condition. In a healthy joint condition, the amplitude of a vibration waveform is normally distributed. Thus, the variance will be larger. The variance is calculated as

$$\sigma^2=\frac{1}{t_2-t_1}\int_{t_1}^{t_2}[y(t)-\mu_y]^2\,\mathrm{d}t, \quad (6)$$

where $[t_1{:}t_2]$ is the time interval of the reversal of motion, $y(t)$ is the vibration waveform, and μ_y is the mean value of the waveform during $[t_1{:}t_2]$.

2.2.2. *Kurtosis (during the interval of motion reversal)*

High kurtosis values will be obtained if the original time waveform is of an impulsive nature [16]. It is defined as

$$Kur=\frac{1}{\sigma^4(t_2-t_1)}\int_{t_1}^{t_2}[y(t)-\mu_y]^4\,\mathrm{d}t. \quad (7)$$

2.2.3. *Peak amplitude (during the interval of the reversal of motion)*

$$y_{\max}=\max\{y(t)\},\quad t_1\leqslant t\leqslant t_2. \quad (8)$$

It is important to determine backlash, especially when y is an acceleration.

2.2.4. *Energy (for the whole transient duration)*

It can be defined as

$$E_h=\int_0^{t_c}y^2(t)\,\mathrm{d}t, \quad (9)$$

where t_c is the duration of one cycle signature.

2.2.5. *Local energy (during the interval of the reversal of motion, and in a certain frequency range)*

It is worthwhile considering the local energy in a subregion of a TF plane as a feature by examining the fact that it can exhibit differences for various fault conditions.

$$E_p = \int_{t_1}^{t_2} \int_{f_1}^{f_2} T(t, f)\, \mathrm{d}f\, \mathrm{d}t, \tag{10}$$

where $T(t, f)$ can be any time–frequency representation, $[t_1{:}t_2]$ and $[f_1{:}f_2]$ are the time interval and the frequency interval of interest. In this study, spectrograms are used, instead of PWVDs or SWVDs, to calculate local energy feature. The reason is that the calculation of spectrograms are more time saving than SWVDs, and the subregions of PWVDs perhaps contain interferences (negative values).

2.3. ARTIFICIAL NEURAL NETWORK

An ANN with supervised learning, based on a modified backpropagation (MBP) algorithm [4], is applied as a pattern recognition tool. The BP algorithm is a gradient descent method that establishes the weights in a multilayer, feedforward adaptive network. Small arbitrary weights are chosen to initialise the system. Learning is accomplished by successively adjusting the weights baesd on one training set each time, i.e. one set of input patterns and the corresponding set of desired output patterns. During this iterative process, an input pattern is presented to the network and propagated forward to determine the result at the output units. The difference between the actual resulting output and the predetermined output in each output unit represents an error that is backpropagated through the network in order to adjust the weightings. The learning process continues until the network responds with outputs the sum of whose square errors from the desired outputs is less than a preset value.

A conventional BP, as described above, has two shortcomings. One is that using one training set to reduce the error in each iteration may misdirect the optimisation path and thus may increase considerably the number of iterations required for convergence. The other is that a constant value of the learning rate (η) may be optimal at one stage of the learning, but there is no guarantee that the same learning rate will be appropriate at any other stage of the learning process.

The following modifications are made to the BP algorithm [4].

- The network weights are not updated after each training set is presented. Rather, the weights are modified only after all the input patterns of training sets have been presented.
- The learning rate is varied according to whether or not an iteration decreases the performance index, i.e. the sum square error for all patterns. If an update results in a reduced error, η is multiplied by a factor $\phi > 1$ for the next iteration. If a step produces a network with an error more than a few (typically, 1–5) per cent above the previous value, all changes to the weights are rejected, η is multiplied by a factor $\beta < 1$, the momentum factor (α) is set to zero, and the step is repeated. When a successful step is then taken, α is reset to its original value.

An ANN architecture consists of the numbers of input nodes (N_i), output nodes (N_o), hidden layers (N_l), and hidden nodes (N_h) in a hidden layer. When using ANNs as tools for fault diagnosis, N_i is decided by the number of the features extracted from original measurement data, N_o is decided by the number of fault types to be detected, and the number of total hidden nodes (N_l and N_h) is up to the degree of complexity in the system

to be diagnosed. In this study, single backlash in joints 6 and 4, and two-joint backlash are detected. Therefore, $N_o = 1$ is used in single backlash detection, and $N_o = 2$ is used in two-joint backlash classification. To quantify the degree of backlash in a joint, the target values of an output node are related to various values during the training phase. The validation performance of trained ANNs is compared by using different network architectures.

3. EXPERIMENTATION AND DATA PROCESSING

The experiments have been conducted on a PUMA 762 industrial robot (Fig. 1). To the purpose for the detection of joint fault, various degrees of backlash are introduced in joints 4 and 6 of the PUMA robot by adjusting the backlash screws of the robot links. These joints are rotational, each of which is driven by a servomotor through a gear train. The vibration responses are measured with an accelerometer mounted at the end effector. From the pattern recognition point of view, multiple-sensor integration is needed to extract enough independent governing features for pattern recognition. If a single-sensor signal contains enough information to distinguish different fault conditions, and each required feature can be extracted through signal processing techniques before the recognition processes, then the condition information via a single sensor can also be considered.

Three types of experiment are performed: (i) with four levels of backlash in joint 6, i.e. zero, small, medium and maximum; (ii) with three levels of backlash in joint 4, i.e. zero, medium and maximum; (iii) with backlash in joints 6 and 4 simultaneously. In addition, the data are collected in two phases: (i) data for the training phase; and (ii) data for the testing (validating) phase. The vibration responses are measured for the following operating conditions (trajectories):

- axis 6, alternating rotation (frequency 2 Hz, angular amplitude 30°);
- axis 4, alternating rotation (frequency 2 Hz, angular amplitude 15°).

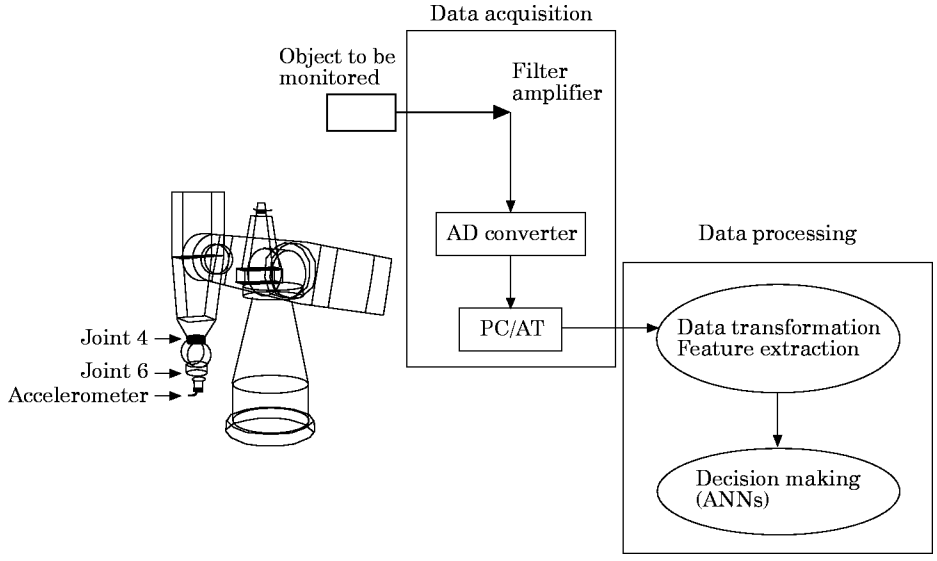

Figure 1. Schematic of experimental set-up.

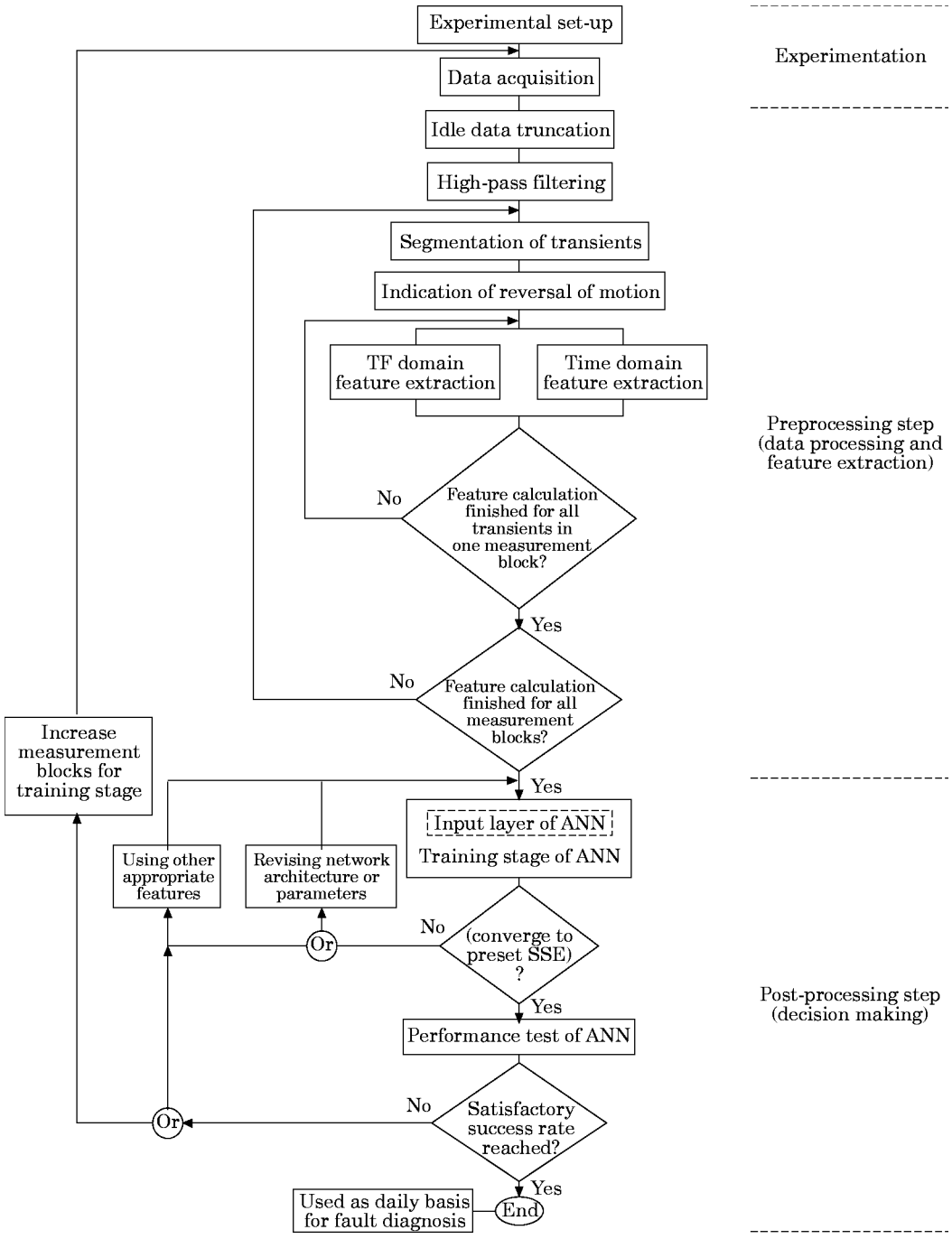

Figure 2. Data processing flow chart for fault diagnosis.

The data acquisition parameters are as follows:

- sampling frequency (f_s): 700 Hz;
- cut-off frequency (f_c): 320 Hz;
- duration of a measurement block (T): 11 s (data for training phase), 3 s (data for testing phase);

- number of measurement blocks (N_m) of the training phase and the testing phase (for each joint condition): 4 and 8 respectively (for single backlash on joint 6); and 5 and 9 respectively (for single backlash on joint 4, and two-joint backlash).

The different fault conditions are denoted as follows:

- Single backlash on joint 6: X_6 (maximum backlash), D_6 (medium backlash), S_6 (small backlash), Z_6 (zero backlash);
- Single backlash on joint 4: X_4 (maximum backlash), D_4 (medium backlash), S_4 (small backlash);
- Backlash on joints 6 and 4: XX (backlash in both joints), XZ (backlash in joint 6), ZX (backlash in joint 4), ZZ (zero backlash).

The data processing flow chart for joint fault diagnosis of the robot is illustrated in Fig. 2, although it can also be applied for fault diagnosis in general. Every acceleration signal is digitally high-pass filtered at 5 Hz to filter out the frequency of the axis rotation (2 Hz) which would otherwise dominate the vibration spectrum. From a global point of view the vibration response seems to be periodical because the robot links rotate with constant frequency; but when looking into a single cycle of response, it is substantially transient. Based on this, 11- and 3-s measurement blocks are segmented into 18 and four transients, respectively (the first and last cycles are discarded). It can be observed (as in Figs 3–5) that the waveform has the lower amplitude at the reversal of motion, i.e. minimum local energy, due to an instant zero speed of the robot link. The impact phenomenon resulting from a backlash is present at the reversal of motion. To indicate

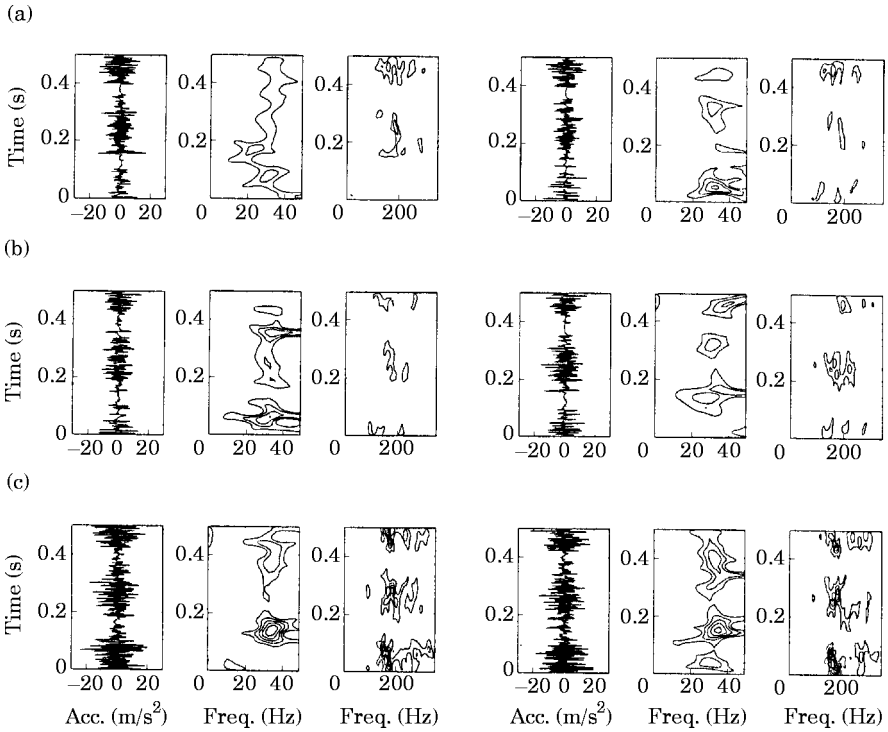

Figure 3. The vibration transients together with their SWVDs for joint 6 backlash (two examples for each fault condition are shown, left and right). (a) X_6, (b) D_6, (c) Z_6. The level values of the SWVD's contour lines: 50, 40, 30, 20, and 10 for the frequency interval 0–50 Hz (1st SWVD in each set of figures); [1600, 1300, 1000, 700, 400 and 100] for the frequency interval 0–350 Hz (2nd SWVD in each set of figures).

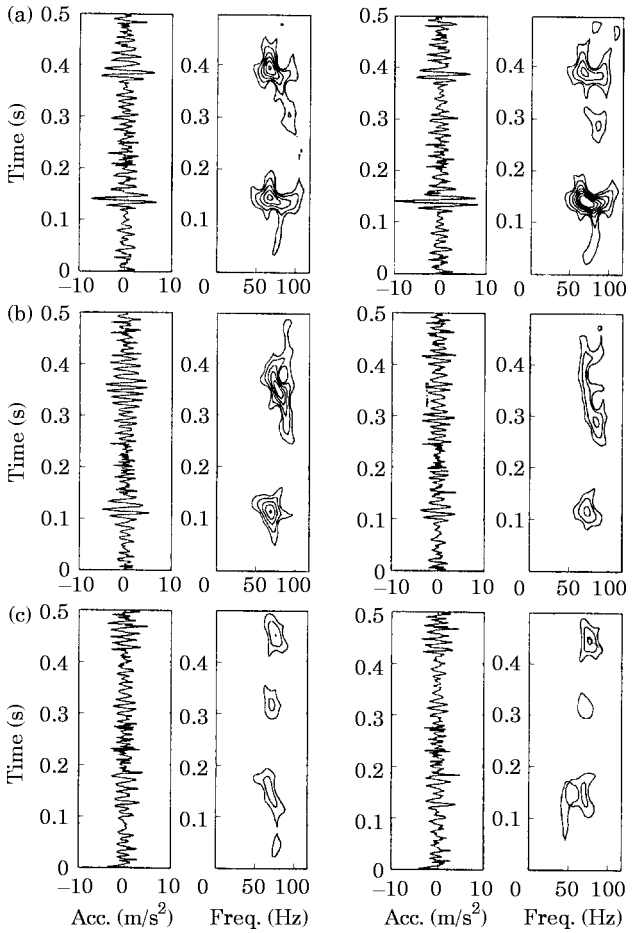

Figure 4. The vibration transients together with their SWVDs for joint 4 backlash (two examples for each fault condition are shown, left and right). (a) X_4, (b) D_4, (c) Z_4. The level values of the SWVD's contour lines: 300, 250, 200, 150, 100, 50 and 20 for the frequency interval 0–120 Hz.

the minimum local energy in a vibration transient, the spectrogram, which proportionally exhibits the energy distribution of a signal in a TF plane, is employed. The location of minimum local energy, which is used for all transients in a measurement block, is detected by taking an average of those locations which are calculated, in the first four transients, respectively, and the time interval, which contains the instant of minimum energy and significant vibration characters, can be set. Therefore, it can be made certain that the impact phenomena are included in the preset time interval if a joint backlash is present.

To use ANNs as tools for pattern recognition, the most relevant features should be extracted from the original transients. However, it is usually difficult to decide what kind of features are the most relevant. To this end, the SWVDs have also been used to help characterise the spectral patterns of the waveforms for different fault conditions. The procedures for TF analysis and feature extraction have been developed in the environment of MATLAB. In Fig. 3, observing the waveforms at the reversal of motion for X_6 or D_6, one can see a zero-acceleration region followed by an impact transient (around 0.1–0.2 s), which is the typical symptom of backlash. This phenomenon is sometimes ambiguous perhaps due to friction on the joint and/or insufficient inertia at the end effector. As to the case Z_6, a resonance around the frequency interval of 25–40 Hz [see the SWVDs of

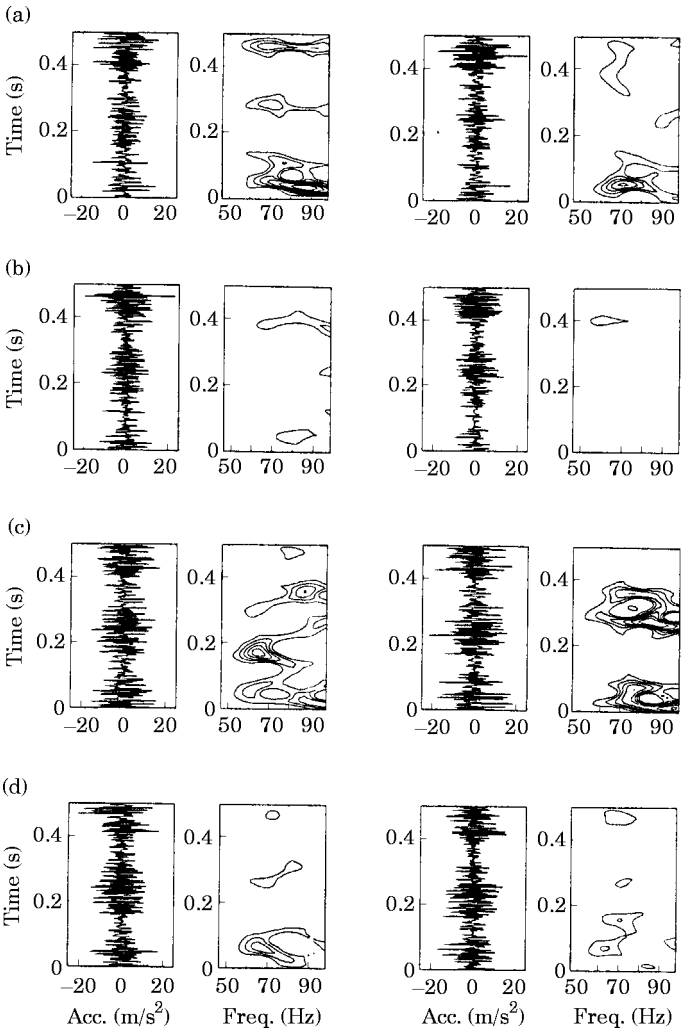

Figure 5. The vibration transients together with their SWVDs for two-joint backlash (two examples for each fault case are shown, left and right). (a) *XX*, (b) *XZ*, (c) *ZX*, (d) *ZZ*. The level values of the SWVD's contour lines: 300, 250, 200, 150, 100 and 50 for the frequency interval 50–100 Hz.

Fig. 3(c)] appears at the reversal of motion, so that no zero-acceleration region can be observed. The possible relevant features for joint 6 backlash are listed in Table 1. In Fig. 4(a), the zero-acceleration regions for the waveforms of fault conditions are slightly corrupted by a resonance with frequency around 70–80 Hz, but the impact peak can still

TABLE 1

Possible relevant features for joint 6 backlash

Notation	Features
$f_{6.1}$	Kurtosis (at the reversal of motion)
$f_{6.2}$	Variance (at the reversal of motion)
$f_{6.3}$	Vibration energy (whole cycle)
$f_{6.4}$	Vibration energy (at the reversal of motion, 25–40 Hz)

TABLE 2

Possible relevant features for joint 4 backlash

Notation	Features
$f_{4,1}$	Kurtosis (at the reversal of motion)
$f_{4,2}$	Variance (at the reversal of motion)
$f_{4,3}$	Vibration energy (whole cycle)
$f_{4,4}$	Peak amplitude (at the reversal of motion)

be observed clearly. The possible relevant features for joint 4 backlash are listed in Table 2. It can be observed that the vibration levels for the joint 6 cases are apparently higher than those for the joint 4 cases (see the level values of SWVDs contour lines in Figs 3 and 4). One can conclude that the vibration due to the motion of joint 6 will dominate the whole waveforms in two-joint backlash conditions. The differences between the energy distribution of this subregion for different faults in the range 50–100 Hz are distinct (Fig. 5). A few possible relevant features are listed in Table 3. The relationship between features and fault conditions, i.e. the mean values and the standard deviations of features for single and two-joint backlash, are shown in Figs 6–8.

In the training phase and the validating phase of ANNs, the use of different numbers of features, which define the number of input nodes (N_i), and the use of different numbers of hidden nodes (N_h) are compared to see the performance of the ANNs. The networks used for this study are designed and trained by using the neural network toolbox of the MATLAB package. The calculation parameters are set as $\alpha = 0.95$, $\eta = 0.1$, $\phi = 1.05$ and

TABLE 3

Possible relevant features for two-joint backlash

Notation	Features
$f_{46,1}$	Kurtosis (at the reversal of motion)
$f_{46,2}$	Variance (at the reversal of motion)
$f_{46,3}$	Vibration energy (whole cycle)
$f_{46,4}$	Vibration energy (at the reversal of motion, 25–40 Hz)
$f_{46,5}$	Peak amplitude (at the reversal of motion)

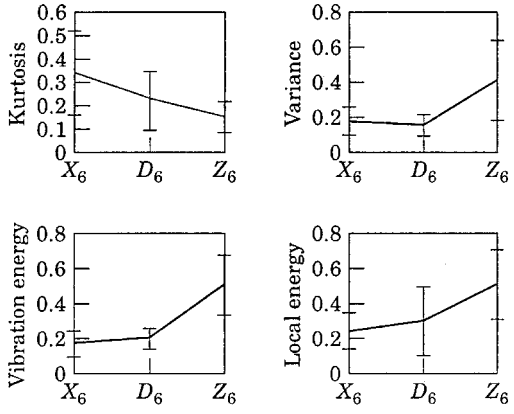

Figure 6. The relationship between features and fault conditions for joint 6.

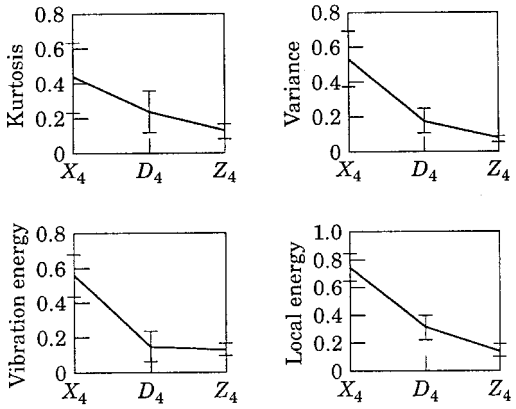

Figure 7. The relationship between features and fault conditions for joint 4.

$\beta = 0.7$, the definition of which are addressed in the previous section. All the input data of an ANN in the training phase are normalised between 0.05 and 0.95 as [17]

$$V_n = \frac{0.9(V - V_{\min})}{V_{\max} - V_{\min}} + 0.05, \tag{11}$$

where $V_{\max}$ and $V_{\min}$ are the maximum and minimum values of that training feature, and V denotes the training features to be normalised. In the validating phase, the input of the ANNs are still normalised by equation (11), where V denotes the validating features in this circumstance. The normalised values are set as 0.95 or 0.05 when the validating features are larger or smaller than the corresponding $V_{\max}$ and $V_{\min}$ in the training phase. Hence, the saturation phenomena during the calculation of sigmoid functions can be avoided.

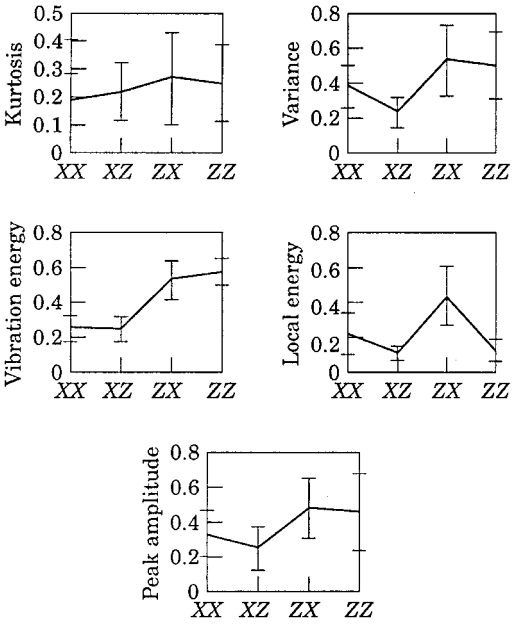

Figure 8. The relationship between features and fault conditions for two-joint backlash.

3.1. *Single backlash in joint 6*

For each joint condition, the training features are extracted from four 11-s measurement blocks (with 18 transients for each block), so that there are 72 transients (and also 72 sets of features) for one condition. The data acquired from the X_6 and N_6 conditions are collected as a training base. According to the relationship between features and fault conditions (Fig. 6), all combinations of two from four possible relevant features (Table 1) are presented to the different ANNs. That is to say, the number of input nodes (N_i) is 2. The mean of three values of a feature ($N_{avg} = 3$) composes a training set. Therefore, 24 ($72/N_{avg}$) training sets are obtained from each joint condition, which satisfy the minimum number of training sets to be used [18], i.e.

$$N = 2(N_i + 1), \tag{12}$$

where N is the number of training sets. During the training phase, the target output of a training set is specified as 0.95 for the backlash condition, and 0.05 for zero-backlash condition. Four kinds of joint conditions (X_6, D_6, S_6 and Z_6) are used to test the detection performance of an ANN. The validating data are extracted from 32 3-s measurement blocks (eight blocks for each condition) with four transients per block. If the output value of the trained ANN for a set of validating data is larger than 0.5, it is judged as a backlash case; otherwise, it is seen as still in normal condition. It can be seen that the $2 \times 6 \times 1$ neural net structure with features f_{6_1} and f_{6_3} yields the best detection performance for single backlash in joint 6 (Table 4).

3.2. *Single backlash in joint 4*

For each joint condition, the training features are extracted from five 11-s measurement blocks (with 18 transients per block), so that there are 90 transients (also 90 sets of features)

TABLE 4

A list of success rate for joint 6 backlash

Feature used	No. of hidden nodes	No. of faulty conditions detected correctly				No. of successful samples (total 128)	Success rate (%)
		X_6	D_6	S_6	Z_6		
(f_{6_1}, f_{6_2})	2	30	19	8	32	89	69.5
	4	30	19	8	32	89	69.5
	6	30	19	8	32	89	69.5
(f_{6_1}, f_{6_3})	2	32	26	29	32	119	93.0
	4	32	26	27	32	117	91.4
	6	32	30	31	32	125	97.7
(f_{6_1}, f_{6_4})	2	31	21	17	26	95	74.2
	4	31	21	14	32	98	76.6
	6	31	21	17	29	98	76.6
(f_{6_2}, f_{6_3})	2	32	32	32	14	110	85.9
	4	32	31	32	17	112	87.5
	6	32	32	32	14	110	85.9
(f_{6_2}, f_{6_4})	2	32	25	22	18	97	75.8
	4	32	25	22	18	97	75.8
	6	32	25	22	19	98	76.6
(f_{6_3}, f_{6_4})	2	32	28	28	19	107	83.6
	4	32	29	29	19	109	85.2
	6	32	28	28	16	104	81.3

32 testing samples per condition.

for one condition. Similarly, the data acquired from the X_4 and Z_4 conditions are collected as a training base. All combinations of two from four possible relevant features are used to present into ANNs, i.e. $N_i = 2$. The mean of three values of a feature ($N_{avg} = 3$) composes a training set. Therefore, 30 ($90/N_{avg}$) training sets are obtained from each joint condition, which satisfy the condition of equation (12). During the training phase, the target output of a training set is specified as 0.95 or 0.05 for backlash, or normal condition, respectively. Two kinds of joint faults, X_4 and Z_4, are used to evaluate the classification performance of the trained ANN. The validating data are extracted from 36 3-s measurement blocks (nine for each condition) with four transients per block. If the output value of a set of validating data is larger than 0.5, it is judged as a backlash case; otherwise, it is seen as belonging to the class of normal condition. The result of using different features and network structures is that it is quite successful to detect the X_4 and Z_4 condition (Table 5). However, the fault condition of medium backlash (D_4) cannot be effectively detected. From Fig. 7, it is observed that the values of the mean and the standard deviation for the D_4 and Z_4 conditions are very close to each other. This explains why the medium backlash condition is classified as a zero backlash condition by the trained ANN. Therefore, another procedure is taken to cope with this problem. During the training phase, the features extracted from the signatures of D_4 are also included to compose training sets. Using more training sets can usually generalise the model well, but a more complex network structure is needed to converge to a preset error. The target output of a training set is specified as 0.95, 0.5 or 0.05 for maximum backlash, medium backlash or zero-backlash condition, respectively. Table 6 describes the training parameters, the network structures and the corresponding test performance. Figure 9 shows the output values at the test phase. The test data are extracted from 27 3-s measurement blocks (nine

TABLE 5

A list of success rate for joint 4 backlash

Features used	No. of hidden nodes	No. of faulty conditions detected correctly		No. of successful samples (total 72)	Success rate (%)
		X_4	Z_4		
$(f_{4,1}, f_{4,2})$	2	32	36	68	94.4
	4	30	36	66	91.7
	6	32	36	68	94.4
$(f_{4,1}, f_{4,3})$	2	36	36	72	100
	4	36	36	72	100
	6	36	36	72	100
$(f_{4,1}, f_{4,4})$	2	35	36	71	98.6
	4	35	36	71	98.6
	6	35	36	71	98.6
$(f_{4,2}, f_{4,3})$	2	23	36	59	81.9
	4	24	36	60	83.3
	6	22	36	58	80.6
$(f_{4,2}, f_{4,4})$	2	32	36	68	94.4
	4	31	36	67	93.1
	6	32	36	68	94.4
$(f_{4,3}, f_{4,4})$	2	34	36	70	97.2
	4	36	36	72	100
	6	34	36	70	97.2

36 testing samples for each condition.

TABLE 6

A list of network performance related to training parameters ($f_{4.1}, f_{4.2}$ and $f_{4.4}$ used as features)

N_{avg}	Number of training set	Network structure	Success rate (%)
3	90(30 × 3)	3 × 4 × 1	85.2
2	135(45 × 3)	3 × 6 × 1	88.9
1	270(90 × 3)	3 × 12 × 1	92.6

for each condition) with four transients per block. If a test output of the trained ANN is larger than 0.7, then it is judged to be in the maximum backlash condition (X_4); between 0.4 and 0.7, then it is seen as in medium backlash condition (D_4); and if smaller than 0.4, then it is classified into normal condition. It is found that the network with 3 × 12 × 1 structure (the features $f_{4.1}$, $f_{4.2}$ and $f_{4.4}$ are used, that is to say, an ANN with three input nodes) using 270 training sets yields the most reliable performance.

3.3. *Backlash in two joints*

In this step, four fault conditions, i.e. XX, XZ, ZX and ZZ, are detected and classified for the case of simultaneous backlash in both joints 6 and 4. For each fault condition, the training features are extracted from five 11-s measurement blocks with 18 transients in each block, so that there are 90 transients (and also 90 sets of features) for one condition. The mean of two values of a feature ($N_{avg} = 2$) composes a training set. Namely, 45 ($90/N_{avg}$) training sets are obtained from each joint condition or 180 (45 × 4) in total. The validating data are extracted from nine 3-s measurement blocks (with four transients per block) for each joint condition. Two output nodes are used to express the condition of the joints.

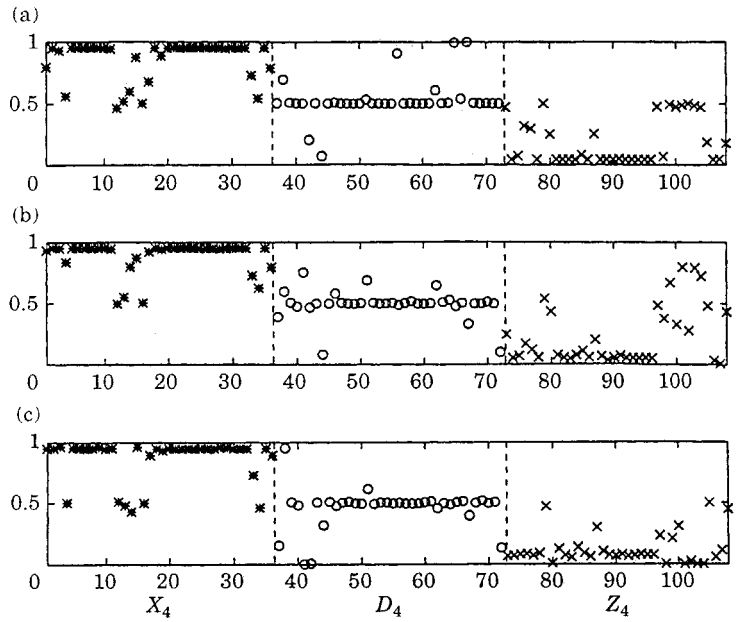

Figure 9. The validating results (output values) using ($f_{4.1}, f_{4.2}, f_{4.4}$) features for joint 4 backlash. (a) $N_h = 4$; (b) $N_h = 6$; (c) $N_h = 12$.

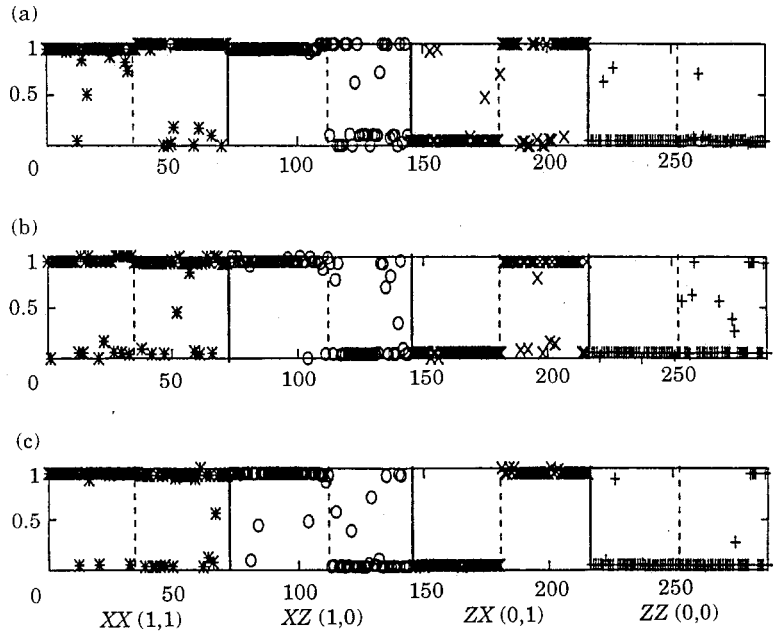

Figure 10. The validating results (output values) using different number of features for two-joint backlash ($N_{h1} = 6$, $N_{h2} = 4$). (a) f_{46_2}, f_{46_3}, f_{46_4}; (b) f_{46_1}, f_{46_2}, f_{46_3}, f_{46_4}; (c) all features.

During the training phase, the target outputs of a training set are specified as 0.95 and 0.05 for the maximum backlash, and zero-backlash conditions, respectively. During the validating phase, if a test output (two values for two output nodes) of the trained ANN is larger than 0.5, then it is in backlash condition for that corresponding joint, otherwise it is classified as normal condition. By calculation , it is found that when using only one hidden layer, the network cannot converge to the preset error value and will not yield good classification performance. From Fig. 8, it can be observed that for each feature, the mean and standard deviation bars of each condition overlap one another. Therefore, a more complex mapping needs to be formulated. A two-hidden-layer structure is considered ($N_{h1} = 6$, $N_{h2} = 4$). By the same procedure, an output value larger than 0.5 is judged as backlash in this joint; otherwise, it is in normal condition. From the output values of ANNs using different number of features, the success rates are 80.6, 86.1 and 88.9%, respectively (Fig. 10). It can be found that using more features helps distinguish subtle differences between fault conditions.

Some general remarks can be given to the training and validating work conducted above.

- The significant features, which make up the training sets, need to be averaged appropriately by choosing an appropriate N_{avg}, due to the uncertainty of the vibration response. For instance, the characteristic of a backlash, a zero-acceleration region followed by an impact transient is sometimes vague, like Fig. 3(a) and (b) show. The features extracted from those bad signatures will make the network hard to converge.
- In the study of single backlash in joints 6 or 4, kurtosis (waveform at the reversal of motion) and vibration energy (the whole transient duration) are the most dominant features which enhance the classification performance of an ANN. As for two-joint backlash, the symptoms of the backlash for joints 6 or 4 are embedded in the waveform resulting from the motion of two joints. Besides, in the particular case considered here,

the vibration energy caused by the motion of joint 4 is relatively small. To distinguish different fault conditions, more features are needed.

- During a training phase, the number of training sets and the number of features are used to constrain sufficiently the training procedure, so that it makes the generalisation behaviour of the pattern classifier acceptable. For instance, using more features helps to generalise the classification model in the two-joint backlash cases. Therefore, using different numbers of features and training sets influence the choice of the number of N_h, and even the number of the hidden layer.

4. CONCLUSIONS

In this paper, an automated robot-joint condition monitoring procedure is proposed. Namely, an ANN approach combined with nonstationary TF analysis is applied to diagnose the joint backlash of an industrial robot. TF analysis is applied in the pre-processing and processing phase and ANNs play the role of tools for pattern classification. A few features of the developed system are as follows.

- The ability to detect automatically the reversal of motion on the robot links is an important ingredient to build an on-line, real-time monitoring system for joint diagnosis of a robot. In this study, non-stationary TF analysis techniques are employed to fulfil this task. The proposed techniques are quite practical and can be applied not only in a well-designed laboratory but also in a real working environment. Although uncertainty exists in operating conditions, system response and measurements, which results in a diversity of vibration waveforms, it is found that the results are still rather satisfactory.
- Very limited instrumentation is used in this work. One sensor is used to detect the fault conditions of two joints. By extracting relevant governing features, and the robust modeling capability of an ANN, various fault conditions can be singled out. In case the vibration level caused by the motion of joint 4 was comparable to that caused by joint 6, the vibration symptoms of the backlash in joint 4 would be more distinct. That is to say, better detection performance can be expected.

ACKNOWLEDGEMENT

This work was partially supported by a grant within the scope of the agreement concluded between the Ministry of Education the Republic of China (Taiwan) and the KU Leuven.

REFERENCES

1. J. Lee and B. M. Kramer 1993 *Journal of Manufacturing Systems* **12**, 379–387. Analysis of machine degradation using a neural network based pattern discrimination model.
2. H. Bicker and A. Daadbin 1989 *Proceedings of ASME 12th Biennial Conference on Mechanical Vibration and Noise*, 273–277. The monitoring of vibration in industrial robots.
3. M. Feldman and S. Braun 1995 *Proceedings of the 13th IMAC*, 637–642. Identification of non-linear system parameters via the instantaneous frequency: application of the Hilbert transform and Wigner–Ville techniques.
4. T. P. Vogl *et al*. 1988 *Biological Cybernetics* **59**, 257–263. Accelerating the convergence of the back-propagation method.
5. L. Cohen 1989 *Proceedings of the IEEE* **77**, 941–981. Time-frequency distributions: a review.
6. F. Hlawatsch and G. F. Boudreaux-Bartels 1992 *IEEE Signal Processing Magazine*, **9**(2), 21–67. Linear and quadratic time-frequency signal representation.

7. M. H. Ackroyd 1971 *Journal of Acoustic Society of America* **50**, 1229–1231. Short-time spectra and time-frequency energy distribution.
8. R. A. Altes 1980 *Journal of Acoustic Society of America* **67**, 1232–1246. Detection, estimation, and classification with spectrogram.
9. T. A. C. M. Classen and W. F. G. Mecklenbrauker 1980 *Philips Journal of Research* **35**, 217–250. The Wigner–Ville distribution—a tool for time frequency signal analysis part I: continuous-time signals.
10. T. A. C. M. Classen and W. F. G. Mecklenbrauker 1980 *Philips Journal of Research* **35**, 276–300. The Wigner–Ville distribution—a tool for time frequency signal analysis part II: discrete-time signals.
11. T. A. C. M. Classen and W. F. G. Mecklenbrauker 1980 *Philips Journal of Research* **35**, 372–389. The Wigner–Ville distribution—a tool for time frequency signal analysis part III: relations with other time-frequency signal transformations.
12. B. Boashash and P. J. Black 1987 *IEEE Transactions on Acoustics*, *Speech*, *and Signal Processing* **35**, 1611–1618. An efficient real-time implementation of the Wigner–Ville distribution.
13. N. D. Cartwright 1976 *Physica* **83**, 210–112. A non-negative quantum mechanical distribution function.
14. A. J. E. M. Janssen and T. A. C. M. Claasen 1985 *IEEE Transactions Acoustic*, *Speech*, *Signal Processing* **33**, 1029–1032. On positivity of time-frequency distributions.
15. M.-C. Pan 1996 *Doctoral Thesis*, *Katholieke Universiteit Leuven*. Non-stationary time-frequency analysis for condition monitoring of mechanical systems.
16. J. Mathew and R. J. Alfredson 1984 *ASME Transactions*, *Journal of Vibration*, *Acoustics*, *Stress and Reliability in Design* **106**, 447–453. The condition monitoring of rolling element bearings using vibration analysis.
17. D. Rumelhart and J. McClelland 1986 *Parallel Distributed Processing 1*. MIT Press.
18. S. Rangwala and D. Dornfeld 1990 *ASME Transactions*, *Journal of Engineering for Industry* **112**, 219–228. Sensor integration using neural networks for intelligent tool condition monitoring.